Available online at www.sciencedirect.com
SCIENCE DIRECT®
Astroparticle Physics 19 (2003) 329–338
Astroparticle Physics
www.elsevier.com/locate/astropart

Measurement of the cosmic ray hadron spectrum up to 30 TeV at mountain altitude: the primary proton spectrum

EAS-TOP Collaboration

M. Aglietta [a,b], B. Alessandro [b], P. Antonioli [c], F. Arneodo [d,e], L. Bergamasco [b,f], M. Bertaina [b,f], C. Castagnoli [f], A. Castellina [a,b,*], A. Chiavassa [b,f], G. Cini Castagnoli [b,f], B. D'Ettorre Piazzoli [g], G. Di Sciascio [g], W. Fulgione [a,b], P. Galeotti [b,f], P.L. Ghia [a,b], M. Iacovacci [g], G. Mannocchi [a,b], C. Morello [a,b], G. Navarra [b,f], L. Riccati [b], O. Saavedra [b,f], G.C. Trinchero [a,b], S. Valchierotti [b,f], P. Vallania [a,b], S. Vernetto [a,b], C. Vigorito [b,f]

[a] *Istituto di Fisica dello Spazio Interplanetario, CNR, Torino, I-10133, Italy*
[b] *Istituto Nazionale di Fisica Nucleare, Torino, I-10125, Italy*
[c] *Istituto Nazionale di Fisica Nucleare, Bologna, I-40127, Italy*
[d] *Laboratori Nazionali del Gran Sasso, INFN, Assergi (AQ), I-67010, Italy*
[e] *Dipartimento di Fisica dell' Università, L'Aquila, I-67100, Italy*
[f] *Dipartimento di Fisica Generale dell' Università, Torino, I-10125, Italy*
[g] *Dipartimento di Scienze Fisiche dell' Università and INFN, Napoli, I-80126, Italy*

Received 1 March 2002; received in revised form 24 July 2002; accepted 3 August 2002

Abstract

The flux of cosmic ray hadrons at the atmospheric depth of 820 $g\,cm^{-2}$ has been measured by means of the EAS-TOP hadron calorimeter (Campo Imperatore, National Gran Sasso Laboratories, 2005 m a.s.l.).

The hadron spectrum is well described by a single power law:

$$S_h(E_h) = (2.25 \pm 0.21 \pm 0.34^{sys}) \times 10^{-7} \left(\frac{E_h}{1000}\right)^{(-2.79\pm0.05)} \quad m^{-2}\,s^{-1}\,sr^{-1}\,GeV^{-1}$$

overthe energy range 30 GeV–30 TeV. The procedure and the accuracy of the measurement are discussed.

The primary proton spectrum is derived from the data by using the CORSIKA/QGSJET code to compute the local hadron flux as a function of the primary proton spectrum and to calculate and subtract the heavy nuclei contribution (basing on direct measurements). Over a wide energy range $E_0 = 0.5$–50 TeV its best fit is given by a single power law:

$$S(E_0) = (9.8 \pm 1.1 \pm 1.6^{sys}) \times 10^{-5} \left(\frac{E_0}{1000}\right)^{(-2.80\pm0.06)} \quad m^{-2}\,s^{-1}\,sr^{-1}\,GeV^{-1}$$

* Corresponding author. Address: Instituto di Fisica della Spazio Interplanetario del CNR, Corso Fiume 4, Torino 10133, Italy. Tel.: +39-11-6306810; fax: +39-11-6604056.
E-mail address: castelli@to.infn.it (A. Castellina).

0927-6505/03/$ - see front matter
doi:10.1016/S0927-6505(03)00103-8

The validity of the CORSIKA/QGSJET code for such application has been checked using the EAS-TOP and KASCADE experimental data by reproducing the ratio of the measured hadron fluxes at the two experimental depths (820 and 1030 g cm^{-2} respectively) at better than 10% in the considered energy range.

PACS: 96.40.Pq; 96.40.De; 29.40.Vj
Keywords: Cosmic rays; Hadrons; Primary protons; High energy calorimetry

1. Introduction

The spectrum of hadrons detected at different atmospheric altitudes retains significant information about the energy/nucleon spectrum of primary cosmic rays, which is dominated by the lightest component, i.e. the proton one. Its measurement has been carried on in the past, both at sea level [1–6] and at mountain altitude [7–11], using different experimental techniques, like emulsion chambers, magnetic spectrometers and calorimeters.

The knowledge of the primary proton spectrum is of main relevance for the understanding of the cosmic rays acceleration mechanisms and of the propagation processes in the Galaxy. Moreover, the proton component is mainly responsible for the uncorrelated particle production in the atmosphere: any uncertainties on the proton spectrum reflect in an uncertainty in the calculation of the secondary particle fluxes (π and K) and thus, for example, on the knowledge of the atmospheric muon and neutrino fluxes. A precise knowledge of such spectra is of particular importance to interpret the observational data from muon and neutrino detectors deep underground [12].

The measurement of the primary proton spectrum has been performed by means of satellite and balloon borne experiments [13–26,39] and indirectly derived by using ground based detectors [27–30]. In the region of tens of TeV, however, direct measurements lack statistics; moreover their energy determinations are not calorimetric and depend on the interaction parameters and their fluctuations. The data inferred from hadron measurements at ground level can therefore provide significant new information.

On the other side, the derivation of the information on the primary cosmic ray spectrum from hadron measurements, as well as the comparison of the results from different experiments, relies on the use of simulation tools describing the interaction and propagation of primary cosmic rays in the atmosphere. The response of such hadron interaction models has therefore to be verified, especially considering that the recorded hadrons are the results of large fluctuations with respect to the average behavior.

The EAS-TOP Extensive Air Shower array was located at Campo Imperatore, 2005 m a.s.l, above the underground Gran Sasso Laboratories, with the aim of studying the cosmic ray spectrum in the energy range 10^{13}–10^{16} eV through the detection of the different air shower components.

In this paper, we present and discuss the results obtained in the study of the uncorrelated hadrons by means of the calorimeter of EAS-TOP, namely:

(a) the measurement of the hadron flux in the energy range 30 GeV–30 TeV;
(b) the derivation of the primary proton energy spectrum in the range 0.5–50 TeV;
(c) the check of the propagation and interaction code (CORSIKA/QGSJET) used for the interpretation of the data.

2. The detector and the hadron trigger

The Muon and Hadron Detector of EAS-TOP is a 144 m^2 calorimeter [31] made of nine layers, each composed by a 13 cm iron slab absorber (except for the uppermost plane which is unshielded), and three planes of limited streamer tubes, for a total depth of 818.5 g cm^{-2}.

Two of the streamer tube layers (with 100 μm wire diameter at 4650 V) act as tracking devices, and are read by a two-dimensional system based

on the anode wires and external orthogonal pick up strips. The third one, which data are used for the present analysis, operates in saturated proportional mode (the wire diameter being 50 μm, and the HV at 2900 V) for hadron calorimetry and EAS core studies. The signal charges are collected by a matrix of 840 (40×38) cm^2 pads placed above the tubes; the pad signals are transferred to charge integrating ADCs with 15 bit dynamic range. The pad read-out is converted to the equivalent number of vertical particles by means of periodical calibration runs based on single muon triggers (pressure and temperature dependence of the induced charge being corrected for).

Different sets of scintillators are placed in the apparatus for different aims; in particular, of the six ones lodged below the second absorber layer, three are used for hadronic trigger purposes. Each scintillator, of dimensions (80×80) cm^2, is centered on a pad, viewed by two identical photomultipliers operating in coincidence and discriminated at the level of 30 m.i.p., corresponding to the energy loss of a 30 GeV proton incident on the calorimeter. They provide the "local hadron trigger", which generates the read-out of the whole detector. For each scintillator a "tower" is defined, as the stack of 3×3 pads of the eight internal layers centered on the scintillator itself. The detector and its operation are fully described in Ref. [31]; a scheme of a "tower" is shown in Fig. 1.

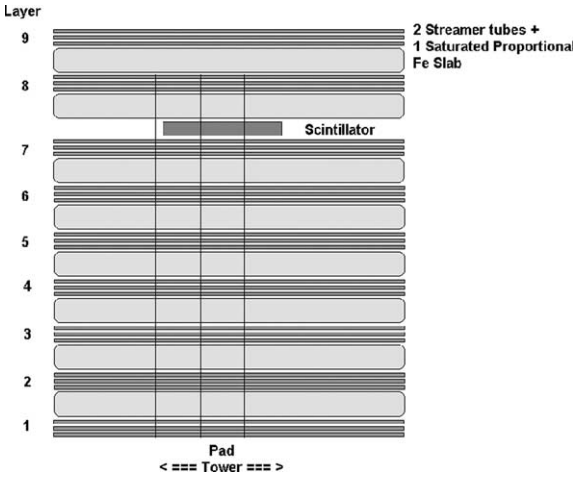

Fig. 1. Schematic view showing the plane numbering and one of the defined "towers" inside the EAS-TOP calorimeter.

3. Hadron selection, acceptance and energy calibration

An event, recorded following the "local hadron trigger", is accepted as a hadron if: (a) the cascade crosses at least three consecutive internal layers of the calorimeter, including the one positioned immediately below the triggering scintillator, and (b) the maximum energy release is recorded on the central pad of each plane of the corresponding "tower". This allows the selection of hadrons with energy above 30 GeV, and the definition of the angular acceptance.

The check of hadron selection, the detection efficiency, effective area, angular acceptance, and energy calibration have been obtained by means of simulations of the detector response based on the GEANT code [32] (with FLUKA option for hadronic cascades), including the full description of the apparatus. Protons at fixed primary energy and zenith angle have been generated and analyzed with the same procedure as the experimental data.

Particular care has been put in the modelling of the chamber behavior in the saturated proportional mode; the saturation in the collected charge has been studied in detail and included in the simulation, as fully discussed in [31]. The modelling of the chamber response to large particle densities has been checked at the 50 GeV e^+ beam at CERN-PS, using a detector built by chambers with the same characteristics, read-out and filling gas mixture as the ones operating on site, but with length reduced to 3 m. Lead was used as absorber in front of the chambers in order to reach maximum particle density [31]. The chamber response was tested and found to agree with the model inside 2% up to particle densities $\rho_{ch} \simeq 300$ particles cm^{-2}, corresponding to a 50 GeV electromagnetic shower after 4 cm of lead absorber. For iron absorber and the calorimeter geometry such particle density corresponds to hadrons with energy $E_h \simeq 650$ GeV.

Such response, introduced in the quoted simulation, provides transition curves that can be

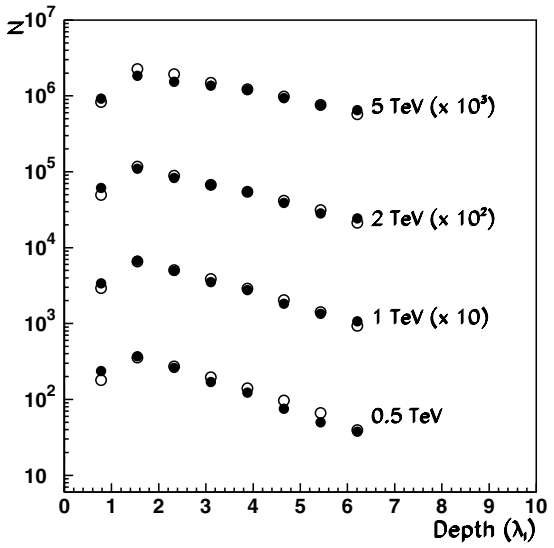

Fig. 2. Mean transition curves for hadrons in the calorimeter. (●) experimental data; (○) simulation.

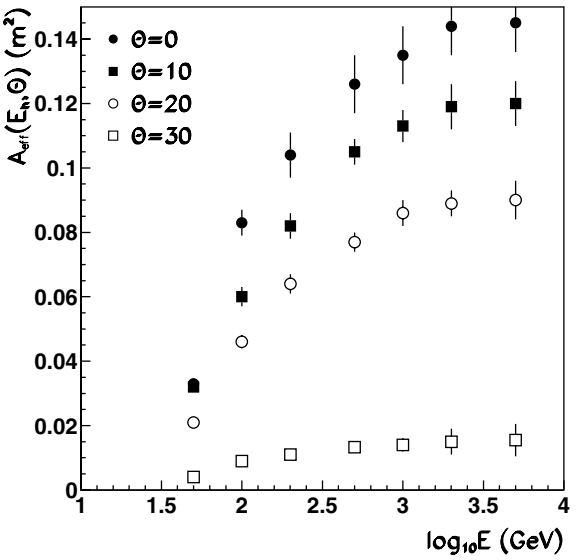

Fig. 3. Effective area $A_{\rm eff}(E_{\rm h},\theta)$ for each "tower" versus $\log_{10} E_{\rm h}$ for four different hadron incidence angles.

directly compared with the experimental data. As shown in Fig. 2, the difference between the two curves is always less than 10% even at shower maximum, where the particle density is the highest, thus showing that the chamber behavior and saturation are well described at least up to 5 TeV (i.e. at particles densities at which the chamber response could not be directly tested).

The verification of the hadron selection procedure has been performed by comparing the shapes of the longitudinal developments for individual events with the expectations from the simulated ones (the agreement on the average transition curves having been shown in Fig. 2). For layers 1–7 (i.e. the ones shielded by more than two iron slabs, see Fig. 1) the experimental and simulated $N_{\rm l}/N_{\rm tot}$ distributions (i.e. the ratio between the equivalent particle number recorded in each layer and the total one in the tower) are in agreement inside the statistical errors ($\simeq$10%). For layer 8 (shielded by a single iron slab), the contamination from the accompanying shower adds an excess of 15% of $N_{\rm tot}$ in 16% of the events, independent on $N_{\rm tot}$. The effect does not alter the hadron selection and the spectrum measurement beyond the systematic effects discussed in the following.

For the described triggering conditions, the effective area $A_{\rm eff}(E_{\rm h},0)$ was determined using the same simulation code and taking into account the inefficiency of the trigger scintillators due to the 30 m.i.p. threshold. Such area includes the detection efficiency, which, concerning energy, rises above 65% at $E_{\rm h} \simeq 130$ GeV for vertical incidence inside the geometrical area of the central pad. As regards zenith angle, the efficiency at 30° is about 10% of the vertical one. The selection condition therefore introduces a cut in the angular acceptance such that 90% of the events are found inside 22° from the vertical direction.

The effective area of each "tower" is shown in Fig. 3 for four different zenith angles.

The hadron energy is inferred from the total charge induced on the eight shielded layers of the defined "tower" (more than 95% of the shower particles at all energies are contained inside a 20 cm radius from the hadron position).

The conversion curve from the total number of particles induced in the "tower" ($N_{\rm tot}$) to the primary hadron energy is shown in Fig. 4. The energy resolution is a $\sigma(E_{\rm h})/E_{\rm h} = 15\%$ at 1 TeV, worsening to 25% at 5 TeV due to leakage losses and to 30% at 30 GeV due to sampling losses. The de-

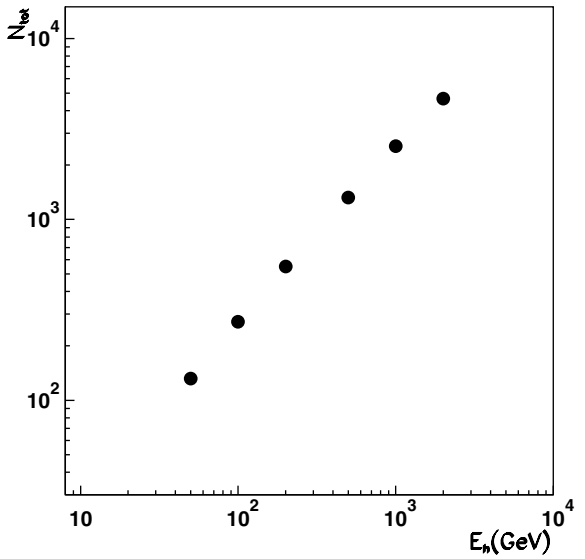

Fig. 4. Total number of induced equivalent particles versus primary energy.

pendence of the total number of particles on the hadron zenith angle is less than 3% up to 30°; the difference in the conversion curve between protons and pions impinging on the calorimeter is less than 2%.

The possibility that the triggering and selection procedure includes more hadrons has been studied by means of a simulation of cascades in the atmosphere through CORSIKA/QGSJET. It results that such hadron pile-up effect, even at the highest energies ($E_h > 3$ TeV), does not alter the average energy determination of more than 6%. As a test, to evaluate possible contaminations from the accompanying shower particles, the particle–energy conversion curve has also been obtained using the total charge induced on the five innermost planes only. No statistically significant difference was found in the hadron fluxes obtained in the two cases over the considered energy range.

4. The hadron flux

About one million triggers were recorded in $T = 14760$ h of effective live time used in the present analysis; 40 832 of them survived the selection criteria and were classified as hadrons.

The measured number of events in each energy bin for the flux $S(E,\theta)$ is:

$$n_{ev}^{meas}(E_h\text{–}E_h + \Delta E_h) = \int_0^{\Omega}\int_{E_h}^{E_h+\Delta E_h} S(E,\theta) T A_{eff} \times (E,\theta)\,d\Omega\,dE \quad (1)$$

The hadron flux at zenithal angle θ can be approximated as:

$$S(E,\theta) = S(E)\exp\left[-\frac{x(\theta)-x}{\Lambda(E)}\right] \quad (2)$$

where $S(E)$ is the flux in vertical direction and $x(\theta)$ is the atmospheric depth along θ. The attenuation length $\Lambda(E)$ has been derived using the CORSIKA [33] code to simulate the interactions and propagation of primary protons in air. In fact the hadron flux in the atmosphere includes both residual primaries and secondaries; at the EAS-TOP atmospheric depth, their ratio rises from $\simeq$0.7 at 500 GeV to $\simeq$1.4 at 5 TeV. Therefore the obtained values of $\Lambda(E)$ represent the full evolution of such mixture: $\Lambda(E) \simeq 114$ g cm^{-2} for QGSJET [34], and $\simeq$131 g cm^{-2} for HDPM [35], for the EAS-TOP altitude and range of zenith angles.

Assuming a power law spectrum ($\gamma = 2.7$) inside each energy bin, the mean value $\overline{E}_h$ is obtained, the corresponding flux being $S(\overline{E}_h) = S(E)(\overline{E}_h/E)^{-\gamma}$ (a change of $\Delta\gamma = 0.1$ in the spectral slope does not produce any appreciable difference in the resulting flux).

The vertical flux is thus:

$$S(\overline{E}_h) = \frac{n_{ev}^{meas}(E_h\text{–}E_h + \Delta E_h)}{2\pi T \overline{E}_h^{\gamma}\int\int E^{-\gamma}\exp\left[-\frac{x(\theta)-x}{\Lambda(E)}\right] A_{eff}(E,\theta)\sin\theta\,d\theta\,dE} \quad (3)$$

The recorded number of events and the experimental hadron fluxes at the atmospheric depth of 820 g cm^{-2} are listed in Table 1 with the corresponding statistical uncertainties.

The following sources of systematic uncertainties have to be considered:

1. The uncertainty in the evaluation of the effective area, $\delta A_{eff}/A_{eff} \simeq 12\%$ at all energies.

Table 1
The measured hadron flux at 820 g cm^{-2}

Mean energy (GeV)	E_0 (GeV)	E_1 (GeV)	Hadron numbers	S_{had} (m^2 s sr GeV)$^{-1}$	$\sigma(S_{had})$ (m^2 s sr GeV)$^{-1}$
41	32	56	10 222	0.12×10^{-2}	0.12×10^{-4}
73	56	100	12 875	0.27×10^{-3}	0.24×10^{-5}
129	100	178	9506	0.60×10^{-4}	0.63×10^{-6}
229	178	316	4930	0.14×10^{-4}	0.21×10^{-6}
408	316	562	2174	0.29×10^{-5}	0.66×10^{-7}
726	562	1000	802	0.47×10^{-6}	0.18×10^{-7}
1290	1000	1778	299	0.92×10^{-7}	0.56×10^{-8}
2295	1778	3162	119	0.17×10^{-7}	0.16×10^{-8}
4081	3162	5623	44	0.26×10^{-8}	0.46×10^{-9}
7257	5623	10 000	23	0.84×10^{-9}	0.18×10^{-9}
12 904	10 000	17 783	12	0.14×10^{-9}	0.49×10^{-10}
22 945	17 783	31 623	3	0.55×10^{-10}	0.39×10^{-10}

The given uncertainties are the statistical ones.

2. The uncertainty in the hadron angular distribution, which reflects in the evaluation of the attenuation length $\Lambda(E)$. A comparison between two different models (QGSJET and HDPM) in the CORSIKA frame shows that the differences in $\Lambda(E)$ reflect in a flux uncertainty $\delta S/S \simeq 5\%$.
3. The uncertainty in the energy assignment to each single hadron, for a spectral slope $\gamma \simeq 2.7$, results in a flux uncertainty $\delta S/S \simeq 7\%$. This value reaches 10% at the highest energies, as shown by the comparison of the measured and simulated longitudinal shower profiles.
4. An uncertainty $\delta S/S \simeq 15\%$ on the flux, due to the different behavior and efficiency of the triggering scintillators and to the different calibrations and stability of the corresponding "towers".

A total systematic energy dependent uncertainty $\delta S/S \simeq 15\%$ is obtained from the first three items. To this, the 15% constant systematic uncertainty due to item 4 has to be added.

The hadron flux is fitted by a power law from 30 GeV up to 30 TeV as

$$S_h(E_h) = (2.25 \pm 0.21) \times 10^{-7} \times \left(\frac{E_h}{1000}\right)^{(-2.79\pm0.05)} \text{m}^{-2}\,\text{s}^{-1}\,\text{sr}^{-1}\,\text{GeV}^{-1} \quad (4)$$

with $\chi^2 = 0.91$ and is shown in Fig. 5.

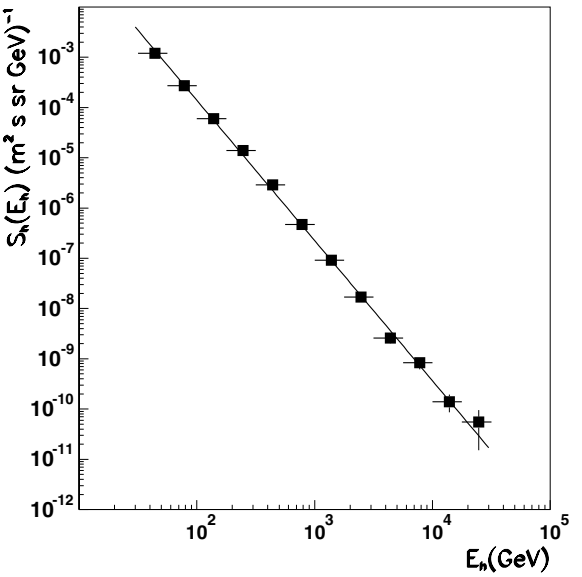

Fig. 5. The hadron flux at 820 g cm^{-2}. The best fit (4) is shown superimposed to the data.

In the fitting procedure (and in the plot), the energy dependent systematic uncertainties have been included; the 15% energy independent systematic effect has to be added.

The hadron flux is compatible, within the errors, with a single power law. This has been tested by performing the same fit in independent narrower energy ranges, the resulting slopes being shown in Fig. 6.

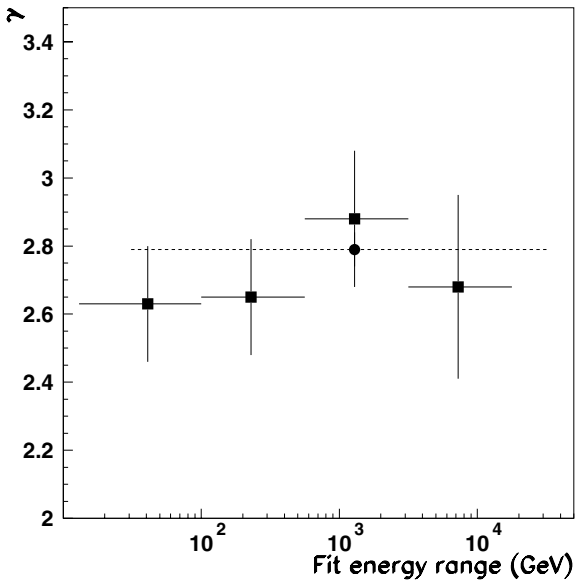

Fig. 6. Slopes of the independent fits to the hadron flux. The fitting energy range is shown. The circle and dashed line show the slope as found in (4).

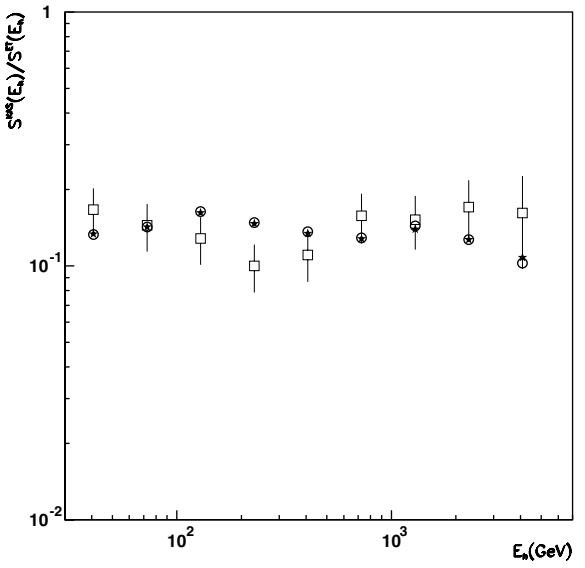

Fig. 7. Ratio of the experimentally measured hadron fluxes by EAS-TOP and KAS-CADE (□) compared to the expectation if the proton + helium primary spectra by JACEE (○) or RUNJOB (★) are assumed.

5. The primary proton spectrum

The primary proton spectrum is derived from the data by:

(a) checking the hadron propagation code in the atmosphere;
(b) subtracting the contribution of heavy primaries from the measured hadron spectrum;
(c) minimizing the difference between the measured and the expected hadron fluxes on the basis of different primary proton spectra.

(a) The region of interest coincides with the energy range in which QGSJET (the hadronic interaction model used to describe the cosmic ray interaction and propagation in the atmosphere) has been directly checked against accelerator data [37,38], both concerning the leading particle and the secondary production physics. Its reliability to reproduce the present data has been checked by comparing its predictions to the measured ratio of hadron fluxes at sea level (KASCADE [36], 1030 $g\,cm^{-2}$) and mountain altitude (EAS-TOP, 820 $g\,cm^{-2}$). Primary protons and helium nuclei were generated in quasi-vertical direction $\theta < 5°$, with energy spectra according to JACEE and RUNJOB [25,26] and the expected hadron fluxes at each observation level were calculated. As shown in Fig. 7, the expected ratio does not depend on the differences between such primary spectra, and it is compatible with the measured one within the statistical uncertainties, the comparison leading to a $\chi^2 = 1.2/\text{d.o.f.}$ On average, the model reproduces the experimental ratio at better than 10%.

We remind that the general features of the model relevant for the calculation of the hadron flux (and therefore object of the test) are the combination of the total cross section and inelasticity for what concerns the contribution of the surviving primaries, and the very forward production cross section for the contribution of the secondaries. We therefore conclude that QGSJET, as implemented in CORSIKA, can be reliably applied in the considered energy range in the description of the uncorrelated hadron fluxes at different atmospheric depths and can be applied

between the top of the atmosphere and the EAS-TOP observation level, thus allowing to derive the primary nucleon flux from the present measurement.

(b) The contribution to the hadron flux from helium primaries has been evaluated using their spectrum as directly measured by the balloon experiments. In order to derive the systematic uncertainties of the procedure, both the RUNJOB ($\gamma_{He} = 2.80$) and JACEE ($\gamma_{He} = 2.68$) data have been used and their contribution subtracted from the experimental hadron flux. At $E_h \simeq 1$ TeV, such contribution is 15% and 29% from RUNJOB and JACEE respectively; the heavier nuclei one is less than 10%.

(c) The primary proton spectrum is obtained as the one minimizing the difference between the measured hadron spectrum (after subtraction of the helium contribution by means of the afore described procedure) and the expected one from simulated proton primaries. Extensive simulations have been carried on, generating primary protons in quasi-vertical direction ($\theta < 5°$), with energy extracted on power law spectra with slope varying between 2.5 and 3.2. The number of simulated events is such that the number of hadrons in each energy bin be much higher than the experimentally collected one. Most of the contribution to each hadron energy bin comes from different primary energy regions; hadrons of energies in different ranges, e.g. $E_h = 0.1$–0.2, 0.2–0.5, 0.5–1, 1–2, 2–5, $\leqslant 5$ TeV are produced by primaries with median energy $E_{MED} \simeq 0.5$, 2, 4, 10, 20, 55 TeV respectively. The data thus allow to get information on the primary proton spectrum in the range 0.5–50 TeV. Assuming a primary spectrum of the power law form $S(E_0) = S_0 E_0^{-\gamma}$, the normalization factor S_0 and the slope γ have been obtained minimizing the differences between the calculated and the measured number of hadrons in each energy bin. The minimizations have been carried on by taking into account both the statistical and the energy dependent systematic uncertainties in the hadron flux.

The data are well described by power law spectra in the energy range 0.5–50 TeV, with best fits, for the case of subtraction of the RUNJOB helium spectrum:

$$S(E_0) = (1.05 \pm 0.16) \times 10^{-4} \times \left(\frac{E_0}{1000}\right)^{(-2.80\pm0.05)} \text{m}^{-2}\,\text{s}^{-1}\,\text{sr}^{-1}\,\text{GeV}^{-1}$$

and for the case of subtraction of the JACEE helium spectrum:

$$S(E_0) = (0.91 \pm 0.15) \times 10^{-4} \times \left(\frac{E_0}{1000}\right)^{(-2.80\pm0.06)} \text{m}^{-2}\,\text{s}^{-1}\,\text{sr}^{-1}\,\text{GeV}^{-1}$$

Including the 7% uncertainty in the helium contribution and the 15% constant systematic uncertainty on the measured hadron flux into a global systematic error term, the result can be summarized as follows:

$$S(E_0) = (9.8 \pm 1.1 \pm 1.6^{\text{sys}}) \times 10^{-5} \times \left(\frac{E_0}{1000}\right)^{(-2.80\pm0.06)} \text{m}^{-2}\,\text{s}^{-1}\,\text{sr}^{-1}\,\text{GeV}^{-1} \quad (5)$$

The obtained proton spectrum is shown in Figs. 8 and 9. The full area and the shaded lines (in the two figures respectively) include the systematic and statistical uncertainties of the measurement.

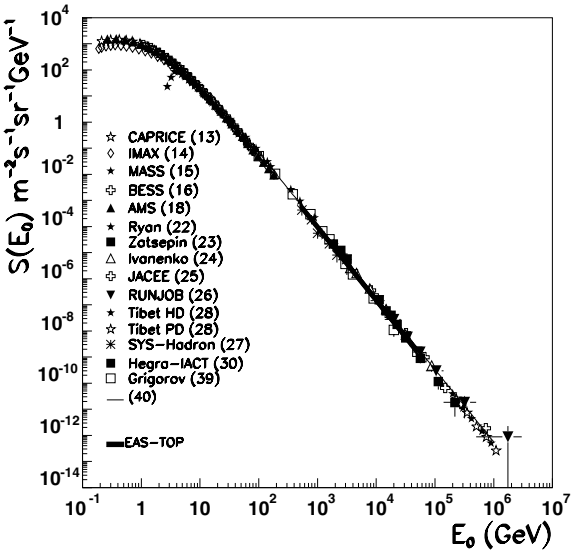

Fig. 8. Primary proton spectrum; the full area represents the result of this measurement and includes the systematic and statistical errors. Results from different experiments are shown for comparison. The straight line represents a fit from [40].

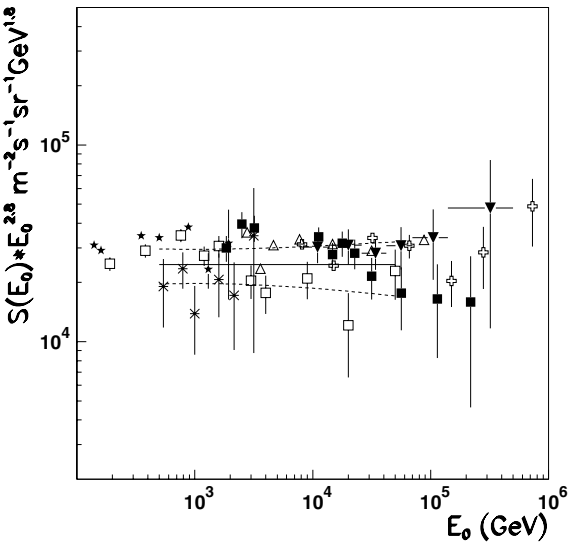

Fig. 9. Primary proton spectrum multiplied by $E_0^{2.8}$. Symbols as in Fig. 8. The horizontal line represents the present result, Eq. (5), with errors.

6. Conclusions

The hadron flux has been measured over a wide energy range (30 GeV–30 TeV) by means of the EAS-TOP hadron calorimeter at the atmospheric depth of 820 $g\,cm^{-2}$. The spectrum is well described by a single power law in the whole range:

$$S(E_h) = (2.25 \pm 0.21 \pm 0.34^{sys}) \times 10^{-7} \times \left(\frac{E_h}{1000}\right)^{(-2.79\pm0.05)} m^{-2}\,s^{-1}\,sr^{-1}\,GeV^{-1}$$

Taking into account the contamination from heavier nuclei, on the basis of direct measurements, the primary proton spectrum is obtained between 0.5 and 50 TeV and is found to be compatible with a single slope power law:

$$S(E_0) = (9.8 \pm 1.1 \pm 1.6^{sys}) \times 10^{-5} \times \left(\frac{E_0}{1000}\right)^{(-2.80\pm0.06)} m^{-2}\,s^{-1}\,sr^{-1}\,GeV^{-1}$$

A systematic uncertainty of about 7% due to the uncertainty in the helium flux is included. The data match very well with the direct measurements over a wide energy range, usually not available to a single experiment, where direct measurements become statistically poor.

The reliability of the CORSIKA/QGSJET interaction and propagation code, which is used to propagate the hadrons in the atmosphere and to compute the heavy nuclei contribution, is directly checked in this energy range by comparison with accelerator data and, concerning the direct application to the present measurement, through its capability to reproduce the ratio of hadron fluxes as measured at two different atmospheric depths by EAS-TOP and KASCADE, at 820 and 1030 $g\,cm^{-2}$ respectively.

Acknowledgements

The cooperation of the Direction and Staff of the Gran Sasso National Laboratories, as well as the technical assistance of C. Barattia, R. Bertoni, G. Giuliani and G. Pirali are gratefully acknowledged.

The comments of an unknown referee have contributed to improve and clarify the text.

References

[1] I.S. Diggory et al., J. Phys. A: Math. Gen. 7 (1974) 741.
[2] G. Brooke, A.W. Wolfendale, Proc. Phys. Soc. 83 (1964) 843.
[3] J. Baruch et al., J. Phys. G: Nucl. Phys. 5 (1979) 595.
[4] R.K. Fickle, R.C. Lamb, Lett. Nuovo Cimento 25 (1979) 289.
[5] F. Ashton, A.J. Saleh, Nature 256 (1975) 387.
[6] E.W. Cowan, K. Matthews, Phys. Rev. D 4 (1971) 37.
[7] M. Amenomori et al., Proc. 18th ICRC, Paris, France 11 (1983) 57.
[8] S.D. Canadov et al., Proc. 19th ICRC, La Jolla, USA 6 (1985) 216.
[9] J.R. Ren et al., Proc. 20th ICRC, Moscow, Russia 5 (1987) 255.
[10] F. Siohan et al., J. Phys. G: Nucl. Phys. 4 (1978) 1169.
[11] D.S. Adamov et al., Proc. 20th ICRC, Moscow, Russia 5 (1987) 464.
[12] A. Castellina, Proceedings of the TAUP 2001 Symposium, LNGS, Italy, Nucl. Phys. B (Proc. Suppl.) 110 (2002) 457.
[13] M. Boezio et al., Astrophys. J. 518 (1999) 457.
[14] W. Menn et al., Astrophys. J. 533 (2000) 281.
[15] R. Bellotti et al., Phys. Rev. D 60 (1999) 052002.
[16] T. Sanuki et al., Proc. 26th ICRC, Salt Lake City, Utah 3 (1999) 93. Available from <astro-ph/0002481>.
[17] W.R. Webber et al., Proc. 20th ICRC, Moscow, Russia 1 (1987) 325.

[18] J. Alcaraz et al., Phys. Lett. B 490 (2000) 27.
[19] S.P. Swordy et al., Proc. 24th ICRC, Rome, Italy 2 (1995) 652.
[20] J. Buckley et al., Astrophys. J. 429 (1994) 736.
[21] E.S. Seo et al., Astrophys. J. 378 (1991) 763.
[22] M.J. Ryan et al., Phys. Rev. Lett. 28 (1972) 985.
[23] V.I. Zatsepin et al., Proc. 23rd ICRC, Calgary, Canada 2 (1993) 13.
[24] I.P. Ivanenko et al., Proc. 23rd ICRC, Calgary, Canada 2 (1993) 17.
[25] K. Asakimori et al., Astrophys. J. 502 (1998) 278.
[26] A.V. Apanasenko et al., Astrophys. Phys. 16 (2001) 13.
[27] N. Inoue et al., Proc. 25th ICRC, Durban, South Africa 4 (1997) 113.
[28] M. Amenomori et al.. Available from <astro-ph/0010292>.
[29] K. Sakurazawa et al., Proc. 25th ICRC, Durban, South Africa 3 (1997) 165.
[30] F. Aharonian et al., Phys. Rev. D 59 (1999) 092003.
[31] R. Adinolfi et al. EAS-TOP Collaboration, Nucl. Instrum. Meth. Phys. Res. A 420 (1999) 117.
[32] Application Software Group and Network Division, GEANT: Detector description and Simulation tool 3.21, CERN W5013, 1994.
[33] D. Heck et al., FZKA 6019, Forschungszentrum Karlsruhe, Germany, 1998.
[34] N.N. Kalmykov, S.S. Ostapchenko, Yad. Fiz. 56 (1993) 105.
[35] J.N. Capdevielle, J. Phys. G: Nucl. Part. Phys. 20 (1994) 637.
[36] H.H. Mielke et al. KASCADE Collaboration, , J. Phys. G: Nucl. Part. Phys. 20 (1994) 637.
[37] R. Engel, Nucl. Phys. B (Proc. Suppl.) 75A (1999) 62.
[38] J. Knapp, Nucl. Phys. B (Proc. Suppl.) 75A (1999) 89.
[39] N.L. Grigorov et al., Proc. 26th ICRC, Salt Lake City, Utah 3 (1999) 183.
[40] B. Wiebel-Sooth et al., Astron. Astrophys. 330 (1998) 389.